Two-Dimensional Convection and Radiation with Scattering from a Poiseuille Flow

M. Kassemi* and B. T. F. Chung†
University of Akron, Akron, Ohio

Two-dimensional combined convection and radiation heat transfer from a gray scattering fluid in a reflecting channel is considered. The model, represented by a set of simultaneous nonlinear integro-partial differential equations, is solved numerically. The effects of aspect ratio, conduction-radiation parameter, scattering albedo, and wall emissivity, are systematically investigated. It is found that these parameters have a significant influence on the temperature field and alter the radiative and convective fluxes at the hot and cold walls. In particular, when radiation effects are considerable, the heat-transfer characteristics of the fluid at the hot and cold walls are very different.

Nomenclature

A = surface area, m^2
g''' = internal heat generation, W/m^3
$\bar{H}$ = width of channel, m
k_t = extinction coefficient, m^{-1}
L = length of channel, m
$\bar{q}$ = dimensionless net radiative heat flux in the medium, $(dQ/dV)/(k_t\sigma T_r^4)$
$\bar{q}_w$ = dimensionless net radiative heat flux at the wall, $(dQ_w/dA)/(\sigma T_r^4)$
T = temperature, K
T_r = reference temperature, K
u = dimensionless velocity, $U/\bar{U}$
$\bar{U}$ = mean velocity, m/s
V = volume, m^3
x,y = dimensionless coordinates, X/L, $Y/\bar{H}$

Dimensionless Parameters

Ar = aspect ratio, $\bar{H}/L$
G = generation number, $g''' \bar{H}/\sigma T_r^4$
N = conduction-radiation parameter, $\lambda(\bar{H}\sigma T_r^3)$
Nu_c = convective Nusselt number, $-(\partial\Theta/\partial y|_w)/(\Theta_w - \bar{\Theta})$
Nu_r = radiative Nusselt number, $\overline{q_w}/N(\Theta_w - \bar{\Theta})$
Pe = Peclet number, $\overline{UH}/\alpha$
τ_o = optical thickness, $k_t\bar{H}$
ε_w = emissivity $(1 - \rho_w)$
α = thermal diffusivity, m^2/s
λ = thermal conductivity, W/m–K
Θ = dimensionless temperature, T/T_r
$\bar{\Theta}$ = dimensionless mixed mean temperature, $\bar{T}/T_r$
σ = Stefan-Boltzmann constant $5.669 \cdot 10^{-8}$, $W/m^2–K^4$

Subscripts

1 = pertaining to bottom wall
2 = pertaining to top wall
e = pertaining to inlet pseudosurface
o = pertaining to outlet pseudosurface
α = denotes sending area
γ = denotes receiving differential volume
μ = denotes sending volume
π = denotes receiving differential area

Introduction

THE study of combined heat transfer from a radiatively participating gray medium has significant applications in furnaces, boilers, nuclear reactors, rocket propulsion systems, plasma generators, and many other high-temperature heat-transfer equipment. Previous investigations in this area have been dominated by one-dimensional analyses of absorbing, emitting media. In the past few years, the effects of two-dimensional radiation,[1] diffuse gray boundaries,[2] and scattering,[1-3] have been studied. In a recent work,[4] in addition to these conditions, nongray effects were also incorporated.

In the present study, the combined effect of laminar convective heat transfer from an absorbing, emitting, isotropically scattering, uniformly heat-generating gray medium subject to two-dimensional radiation is examined. In the present formulation, the boundaries of the channel, which consist of diffuse gray walls, are held at constant but different temperatures. The main objective of this investigation is to study the effects of the relevant parameters of the problem on the temperature distributions in the fluid and to show that under the influence of radiation the heat-transfer characteristics of the hot and cold walls are quite different.

Methods that have been developed for multidimensional radiative transfer can be classified into the approximate techniques,[5] the Monte Carlo method,[6] the zone method,[7] the flux methods,[8] and the finite-element method.[1] The solution method adopted in this investigation is based on an element-to-node generalization of the zone method, which was previously employed to study combined heat transfer of a nonscattering fluid in a black channel.[9] The element-to-node scheme has been modified and extended to include the effects of isotropic scattering and multiple reflections at the diffuse gray walls.

In situations that involve scattering and multiple reflection at the boundaries, the zone method requires the evaluation of total exchange areas. Computation of total exchange areas is a very time-consuming and cumbersome process. As will be seen later, in the present modified scheme, evaluation of total exchange areas is not required. Thus, scattering and multiple reflection problems can be solved with essentially the same computational effort as nonscattering black-boundary cases. Another objective of this paper is to demonstrate the strength, efficiency, and flexibility of this method for solving combined

Received Aug. 9, 1988; revision received Dec. 19, 1988.

*Research Associate, Department of Mechanical Engineering; currently NRC Resident Researcher, NASA Lewis Research Center, Cleveland, Ohio.

†Professor, Department of Mechanical Engineering.

modes of heat-transfer problems that involve isotropic scattering and reflective boundaries. We hope to show that the use of total exchange areas is largely a matter of taste and not a necessity when dealing with this class of problems.

Mathematical Formulation

Consider a hydrodynamically fully developed flow of an emitting, absorbing, isotropically scattering, gray medium in a rectangular channel. The uniformly heat-generating fluid has constant physical properties and is subject to conduction, convection, and two-dimensional radiation. The section under consideration consists of two diffuse, gray parallel walls of finite length and height and infinite width as shown in Fig. 1. These wall sections are held at constant but different temperatures θ_1 and θ_2. The environments exterior to the section at the inlet and outlet are represented by two black sinks.

Striking an energy balance at an infinitesimal fluid volume results in a nonlinear integro-partial differential equation which when set into dimensionless form is given by the following equations:

$$(Ar)(Pe)u\frac{\partial\theta}{\partial x}=\frac{\partial^2\theta}{\partial y^2}-\left(\frac{\tau_o}{N}\right)\bar{q}+\frac{G}{N} \tag{1}$$

The net radiative flux in the medium is defined as

$$\bar{q}=W-H \tag{2a}$$

where the outgoing radiative flux is

$$W=4(1-\omega_o)\theta^4+\omega_o H \tag{2b}$$

and the incident radiative flux is

$$H=\iiint_V W\left(\frac{1}{k_t}\frac{\partial^2 g_\mu g_\gamma}{\partial V\,\partial V_\gamma}\right)\mathrm{d}V+\sum_w^2\iint_{A_w} W_w\left(\frac{1}{k_t}\frac{\partial^2 w_\alpha g_\gamma}{\partial A\,\partial V_\gamma}\right)\mathrm{d}A$$
$$+\iint_{A_e}\theta_e^4\left(\frac{1}{k_t}\frac{\partial^2 s_\alpha g_\gamma}{\partial A\,\partial V_\gamma}\right)\mathrm{d}A+\iint_{A_o}\theta_o^4\left(\frac{1}{k_t}\frac{\partial^2 s_\alpha g_\gamma}{\partial A\,\partial V_\gamma}\right)\mathrm{d}A \tag{2c}$$

A similar radiative balance at the walls results in the following. The net radiative heat flux at the wall is

$$\bar{q}_w=W_w-H_w,\qquad w=1,2 \tag{3a}$$

and the outgoing and incoming radiative fluxes are given by

$$W_W=(1-\rho_w)\theta_w^4+\rho_w H_w,\qquad w=1,2 \tag{3b}$$

$$H_w=\iiint_V W\frac{\partial^2 g_\mu w_\pi}{\partial V\,\partial A_\pi}\mathrm{d}V+\iint_{A_{\bar{w}}} W_{\bar{w}}\frac{\partial^2 w_\alpha w_\pi}{\partial A\,\partial A_\pi}\mathrm{d}A$$
$$+\iint_{A_o}\theta_0^4\frac{\partial^2 s_\alpha w_\pi}{\partial A\,\partial A_\pi}\mathrm{d}A+\iint_{A_e}\theta_e^4\frac{\partial^2 s_\alpha w_\pi}{\partial A\,\partial A_\pi}\mathrm{d}A \tag{3c}$$

where subscripts w and $\bar{w}$ are given by

$w=2,\bar{w}=1$ for top wall

$w=1,\bar{w}=2$ for bottom wall

The radiative exchange factors in the above integral terms are described in Appendix A and Ref. 10, and subscripts e, o refer, respectively, to entrance and exit stations. The scattering albedo of the fluid is given by ω_o, and ρ_w is the reflectivity of the walls. It is assumed that radiation stresses are much smaller than their molecular counterparts. Therefore, they are neglected, and the momentum equation becomes completely decoupled from the energy equation and is readily solved to give the familiar fully developed laminar Poiseuille flow distribution.

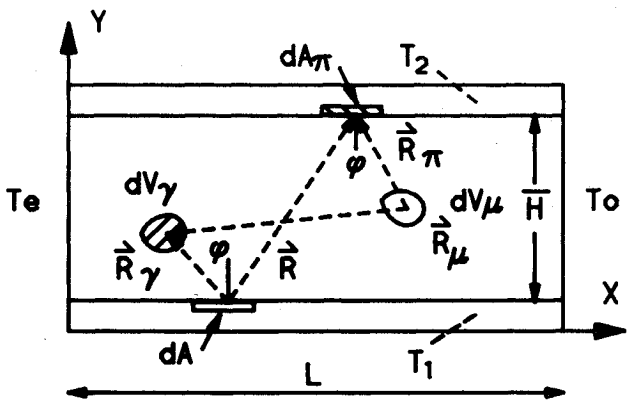

Fig. 1 Cross-sectional view of the rectangular channel section.

$$u=6(y-y^2) \tag{4}$$

The medium is subject to nonslip condition at the wall and prescribed temperature at the inlet

$$\theta=\theta_1,\theta_2 \quad \text{at} \quad y=0,1 \tag{5}$$

$$\theta=\theta_e \quad \text{at} \quad x=0 \tag{6}$$

The latter is also the temperature of the inlet pseudosurface. The temperature of the outlet pseudosurface can be modeled in two ways. In an "open" pipe, that is, when the section exits into a reservoir of known temperature, θ_o is known a priori and, therefore, it can be simply prescribed. But in the present application, we are considering a "heated" section of a channel. Therefore, the temperature θ_o is unknown and cannot be prescribed. Here we follow the example of previous investigators[1,4] in setting θ_o equal to the mixed mean temperature of the fluid at the exit of the section under consideration. In this fashion, θ_o is determined as part of the solution from the expression

$$\theta_o=\frac{\iint_{A_o} u\theta\,\mathrm{d}A}{\iint_{A_o} u\,\mathrm{d}A} \tag{7}$$

If W,H,W_w,H_w are eliminated between Eqs. (2a–2c) and (3a–3c), the result can be written as

1) for the medium

$$\left[\frac{1}{1-\omega_o}\right]\bar{q}-\frac{\omega_o}{4(1-\omega_o)}\iiint_V\bar{q}\left(\frac{1}{k_t}\frac{\partial^2 g_\mu g_\gamma}{\partial V\,\partial V_\gamma}\right)\mathrm{d}V$$
$$-\sum_w^2\left[\frac{\rho_w}{1-\rho_w}\right]\iint_{A_w}\bar{q}_w\left(\frac{1}{k_t}\frac{\partial^2 w_\alpha g_\gamma}{\partial A\,\partial V_\gamma}\right)\mathrm{d}A$$
$$=4\theta^4-\iiint_V\theta^4\left(\frac{1}{k_t}\frac{\partial^2 g_\mu g_\gamma}{\partial V\,\partial V_\gamma}\right)\mathrm{d}V$$
$$-\sum_w^2\iint_{A_w}\theta_w^4\left(\frac{1}{k_t}\frac{\partial^2 w_\alpha g_\gamma}{\partial A\,\partial V_\gamma}\right)\mathrm{d}A$$
$$-\iint_{A_e}\theta_e^4\left(\frac{1}{k_t}\frac{\partial^2 s_\alpha g_\gamma}{\partial A\,\partial V_\gamma}\right)\mathrm{d}A-\iint_{A_o}\theta_o^4\left(\frac{1}{k_t}\frac{\partial^2 s_\alpha g_\gamma}{\partial A\,\partial V_\gamma}\right)\mathrm{d}A \tag{8}$$

2) for the walls

$$\left[\frac{1}{1-\rho_w}\right]\bar{q}_w - \frac{\omega_o}{4(1-\omega_o)}\int\int\int_V \bar{q}\left(\frac{\partial^2 g_\mu w_\pi}{\partial V\,\partial A_\pi}\right)dV - \left[\frac{\rho_{\bar{w}}}{1-\rho_{\bar{w}}}\right]\int\int_{A_{\bar{w}}} \bar{q}_{\bar{w}}\left(\frac{\partial^2 w_\alpha w_\pi}{\partial A\,\partial A_\pi}\right)dA = \theta_w^4 - \int\int\int_V \theta^4\frac{\partial^2 g_\mu w_\pi}{\partial V\,\partial A_\pi}\,dV - \int\int_{A_{\bar{w}}}\theta_{\bar{w}}^4\frac{\partial^2 w_\alpha w_\pi}{\partial A\,\partial A_\pi}\,dA - \int\int_{A_o}\theta_o^4\frac{\partial^2 s_\alpha w_\pi}{\partial A\,\partial A_\pi}\,dA - \int\int_{A_e}\theta_e^4\frac{\partial^2 s_\alpha w_\pi}{\partial A\,\partial A_\pi}\,dA \qquad (9)$$

where subscript w and $\bar{w}$ are defined as before.

Equations (1), (8), and (9) represent the system of integro-partial differential equations that are to be solved for the unknown fluid temperature θ and radiative fluxes $\bar{q}$ and $\bar{q}_w$. These are subject to boundary conditions of Eqs. (5) and (6).

Numerical Formulation

In view of the complexity of the problem, an analytical solution of the governing equations is not feasible, and a numerical approach becomes inevitable. To generate numerical solutions, an element to node approach is adopted. According to this method, the channel is divided into an $\bar{M}\times\bar{N}$ array of rectangular volume elements each centered around a nodal point. Similarly, the two walls are each divided into $\bar{M}$ surface elements, and the two ends are divided into $\bar{N}$ surface elements. This arrangement is shown in Fig. 2. It should be noted that due to the two-dimensional nature of the problem, the region between the walls is infinite in depth; therefore, both the wall and fluid elements depicted are of infinite depth perpendicular to the cross section shown.

Nodal temperature and radiative fluxes are specified at the center of each volume and wall element. Within each volume element a temperature and radiative flux distribution is assumed. These are written in terms of adjacent nodal values according to the following linearized expression:

$$\chi(\eta,\xi) = \chi_{m,n} + (\chi_{m\pm1,n} - \chi_{m,n})\frac{\eta}{\eta_o} + (\chi_{m,n\pm1} - \chi_{m,n})\frac{\xi}{\xi_o} + (\chi_{m\pm1,n\pm1} + \chi_{m,n} - \chi_{m\pm1,n} - \chi_{m,n\pm1})\frac{\eta}{\eta_o}\frac{\xi}{\xi_o} \qquad (10a)$$

where $\chi = \theta^4$, q and η and ξ are local coordinates as shown in Fig. 2. Similarly, within each constant temperature wall element, the radiative flux is given by

$$\bar{q}_w = \bar{q}_{w_m} + [\bar{q}_{w_{m\pm1}} - \bar{q}_{w_m}]\frac{\eta}{\eta_o} \qquad \text{for} \qquad w = 1,2 \qquad (10b)$$

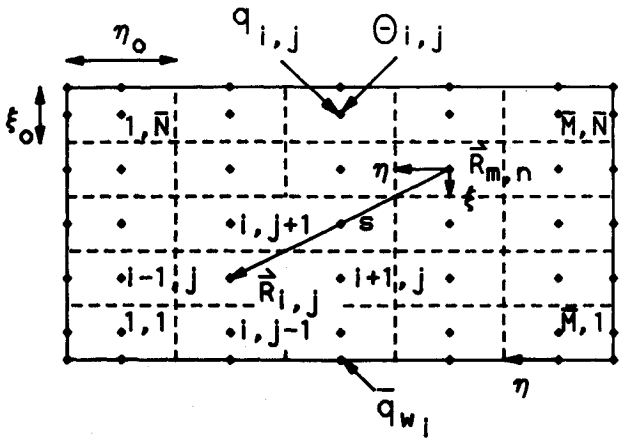

Fig. 2 Grid configuration.

To get the discretized form of the governing equations in terms of nodal temperatures and nodal fluxes, Eqs. (1), (8), and (9) are applied to an infinitesimal volume or area at the center (node) of any element. The derivatives in the conductive and convective terms of Eq. (1) are replaced by their finite-difference representation, and the integrals over the whole domain in Eqs. (8) and (9) are broken into the sum of integrals over each individual element. Finally, substitution of the assumed elemental distributions, Eqs. (10a) and (10b), results in the following set of discretized equations.

$$\frac{G}{N} - (Ar)(Pe)u_{i,j}\left[\frac{\theta_{i,j}-\theta_{i-1,j}}{\Delta x}\right] + \left[\frac{\theta_{i,j+1}-2\theta_{i,j}+\theta_{i,j-1}}{(\Delta y)^2}\right] = \left[\frac{\tau_o}{N}\right]\bar{q}_{i,j} \qquad (11a)$$

and

$$\begin{aligned}
&4\theta_{i,j}^4 - \sum_m^{\bar{M}}\sum_n^{\bar{N}}\theta_{m,n}^4\,\overline{g_{mn}g_{ij}} - \sum_m^{\bar{M}}\sum_n^{\bar{N}}(\theta_{m\pm1,n}^4 - \theta_{m,n}^4)\overline{g_{mn}g_{ij}}' - \sum_m^{\bar{M}}\sum_n^{\bar{N}}(\theta_{m,n\pm1}^4 - \theta_{m,n}^4)\overline{g_{mn}g_{ij}}'' - \sum_m^{\bar{M}}\sum_n^{\bar{N}}(\theta_{m\pm1,n\pm1}^4 + \theta_{m,n}^4 \\
&- \theta_{m\pm1,n}^4 - \theta_{m,n\pm1}^4)\overline{g_{mn}g_{ij}}''' - \sum_w^2\theta_w^4\sum_m^{\bar{M}}\overline{w_m g_{ij}} - \theta_e^4\sum_n^{\bar{N}}\overline{s_{e_n}g_{ij}} - \theta_o^4\sum_n^{\bar{N}}\overline{s_{o_n}g_{ij}}\Big] + \sum_w^2\left[\frac{\rho_w}{1-\rho_w}\right]\Big[\sum_m^{\bar{M}}\bar{q}_{w_m}\overline{w_m g_{ij}} \\
&+ \sum_m^{\bar{M}}(\bar{q}_{w_{m\pm1}} - \bar{q}_{w_m})\overline{w_m g_{ij}}'\Big] \\
&= \left[\frac{1}{1-\omega_o}\right]\bar{q}_{i,j} - \left[\frac{\omega_o}{4(1-\omega_o)}\right]\Big[\sum_m^{\bar{M}}\sum_n^{\bar{N}}\bar{q}_{m,n}\,\overline{g_{mn}g_{ij}} + \sum_m^{\bar{M}}\sum_n^{\bar{N}}(\bar{q}_{m\pm1,n} - \bar{q}_{m,n})\overline{g_{mn}g_{ij}}' + \sum_m^{\bar{M}}\sum_n^{\bar{N}}(\bar{q}_{m,n\pm1} - \bar{q}_{m,n})\overline{g_{mn}g_{ij}}'' \\
&+ \sum_m^{\bar{M}}\sum_n^{\bar{N}}(\bar{q}_{m\pm1,n\pm1} + \bar{q}_{m,n} - \bar{q}_{m\pm1,n} - \bar{q}_{m,n\pm1})\overline{g_{mn}g_{ij}}'''\Big]
\end{aligned} \qquad (11b)$$

Similarly, at walls we have

$$\begin{aligned}
&\left[\frac{1}{1-\rho_w}\right]\bar{q}_{w_i} - \left[\frac{\rho_{\bar{w}}}{1-\rho_{\bar{w}}}\right]\Big[\sum_m^{\bar{M}}\bar{q}_{\bar{w}_m}\overline{w_m w_i} + \sum_m^{\bar{M}}(\bar{q}_{\bar{w}_{m\pm1}} - \bar{q}_{\bar{w}_m})\cdot\overline{w_m w_i}'\Big] = \left[\frac{\omega_o}{4(1-\omega_o)}\right]\Big[\sum_m^{\bar{M}}\sum_n^{\bar{N}}\bar{q}_{m,n}\overline{g_{mn}w_i} + \sum_m^{\bar{M}}\sum_n^{\bar{N}}(\bar{q}_{m\pm1,n} \\
&- \bar{q}_{m,n})\overline{g_{mn}w_i}' + \sum_m^{\bar{M}}\sum_n^{\bar{N}}(\bar{q}_{m,n\pm1} - \bar{q}_{m,n})\overline{g_{mn}w_i}'' + \sum_m^{\bar{M}}\sum_n^{\bar{N}}(\bar{q}_{m\pm1,n\pm1} + \bar{q}_{m,n} - \bar{q}_{m\pm1,n} - \bar{q}_{m,n\pm1})\overline{g_{mn}w_i}'''\Big] \\
&+ \theta_w^4 - \theta_w^4\sum_m^{\bar{M}}\overline{w_m w_i} - \theta_e^4\sum_n^{\bar{N}}\overline{s_{e_n}w_i} - \theta_o^4\sum_n^{\bar{N}}\overline{s_{o_n}w_i} - \sum_m^{\bar{M}}\sum_n^{\bar{N}}\theta_{m,n}^4\overline{g_{mn}w_i} - \sum_m^{\bar{M}}\sum_n^{\bar{N}}(\theta_{m\pm1,n}^4 - \theta_{m,n}^4)\overline{g_{mn}w_i}' \\
&- \sum_m^{\bar{M}}\sum_n^{\bar{N}}(\theta_{m,n\pm1}^4 - \theta_{m,n}^4)\overline{g_{mn}w_i}'' - \sum_m^{\bar{M}}\sum_n^{\bar{N}}(\theta_{m\pm1,n\pm1}^4 + \theta_{m,n}^4 - \theta_{m\pm1,n}^4 - \theta_{m,n\pm1}^4)\overline{g_{mn}w_i}'''
\end{aligned} \qquad (11c)$$

Table 1 Primary direct exchange integrals[a]

$\overline{g_{mn}g_{ij}}$	V_{mn}, s, dV_{ij}	Fluid to fluid: $\frac{2k_t}{\pi}\int_{-\eta_o/2}^{\eta_o/2}\int_{-\xi_o/2}^{\xi_o/2}\frac{F_1(k_ts)}{s}\,d\xi\,d\eta$
$\overline{w_mg_{ij}}$	A_m, s, y_{ij}, dV_{ij}	Wall to fluid: $\frac{2y_{ij}}{\pi}\int_{-\eta_o/2}^{\eta_o/2}\frac{F_2(k_ts)}{s^2}\,d\eta$
$\overline{s_{en}g_{ij}}$	A_n, s, dV_{ij}	Surface to fluid: $\frac{2x_{ij}}{\pi}\int_{-\xi_o/2}^{\xi_o/2}\frac{F_2(k_ts)}{s^2}\,d\xi$
$\overline{s_{on}g_{ij}}$		
$\overline{g_{mn}w_i}$	V_{mn}, s, y_{mn}, dA_i	Fluid to wall: $\frac{2k_t}{\pi}\int_{-\eta_o/2}^{\eta_o/2}\int_{-\xi_o/2}^{\xi_o/2}y_{mn}\frac{F_2(k_ts)}{s^2}\,d\xi\,d\eta$
$\overline{w_mw_i}$	A_m, s, $\bar{H}$, dA_i	Wall to wall: $\frac{2\bar{H}^2}{\pi}\int_{-\eta_o/2}^{\eta_o/2}\frac{F_3(k_ts)}{s^3}\,d\eta$
$\overline{s_{en}w_i}$	A_n, s, y_n, x_i, dA_i	Surface to wall: $\frac{2x_i}{\pi}\int_{-\xi_o/2}^{\xi_o/2}y_n\frac{F_3(k_ts)}{s^3}\,d\xi$
$\overline{s_{on}w_i}$		

[a] $Fp(k_ts)=\int_0^{\pi/2}e^{-k_ts/\cos\phi}(\cos\phi)^{p-1}\,d\phi, \qquad p=1,2,3$

The radiative exchange integrals in the above equations are described in Appendix A and Table 1.

The last unresolved term in the above equations is the exit mixed mean temperature θ_o given by the integral in Eq. (7). To write θ_o in terms of the nodal temperatures, a modified Simpson's integration scheme is employed which conforms with the nonuniformity of the grid at the boundaries.

$$\theta_o=(9/8)u_{\bar{M},1}\theta_{\bar{M},1}+(17/24)u_{\bar{M},2}\theta_{\bar{M},2}+\sum_{n=1}^{N1}u_{\bar{M},2n+1}\theta_{\bar{M},2n+1}+\sum_{n=1}^{N2}u_{\bar{M},2n+2}\theta_{\bar{M},2n+2}+(17/24)u_{\bar{M},\bar{N}-1}\theta_{\bar{M},\bar{N}-1}+(9/8)u_{\bar{M},\bar{N}}\theta_{\bar{M},\bar{N}} \tag{12}$$

where

$$N1=(\bar{N}-3)/2$$

$$N2=(\bar{N}-5)/2$$

Discretization of the governing equations is now complete. Equations (11) and (12) constitute $2\bar{M}(\bar{N}+1)+1$, simultaneous nonlinear equations to be solved for the unknowns, $\theta_{i,j}$, $\bar{q}_{i,j}$, and $\bar{q}_{w_i}$.

The solution procedure is as follows. First, initial trial values for $\theta_{i,j}$ and $\bar{q}_{i,j}$ are chosen. The assumed temperatures $\theta_{i,j}$ are used in Eq. (11a) and $\bar{q}_{i,j}$ are computed. The computed $\bar{q}_{i,j}$ are then substituted into Eqs. (11b) and (11c). The resulting set of algebraic equations are solved iteratively for $\theta_{i,j}$ and $\bar{q}_{w_i}$ using the secant method. This process is repeated until solutions converge according to a predesignated criterion.

The numerical scheme was found to be accurate and extremely efficient. This is mainly due to the existence of the following features.

1) The present approach allows for temperature variation within each element; therefore, it can conveniently deal with problems such as combined heat transfer in which large temperature gradients may be present.

2) Energy conservation is applied to an infinitesimal volume or area. Thus, this scheme is ideal for incorporation into existing codes where conductive and convective terms are represented by finite-difference expressions.

3) In this approach, the direct exchange integrals are evaluated by numerical integration. Although this is a time-consuming process, it has to be performed only once for a given geometry and radiative property. As in the zone method, these quantities can then be stored in tabular form and used with any set of boundary conditions or physical parameters. The flux methods such as the discrete ordinate method do not require computation of direct exchange integrals, but integrate the radiative intensity equation over the incoming direction. These numerical integrations, however, must be repeated whenever a physical parameter or boundary condition is changed.

4) The maximum order of numerical integration for a two-dimensional problem is two. The zone method and the finite-element method each require fourth-order integrations.

5) Unlike the zone method, for cases that involve scattering and reflection at the boundaries, the present scheme does not require the computation of total exchange areas. Total exchange areas are usually computed by either the nonexplicit scalar procedure presented in Ref. 7 or by the explicit matrix approach promulgated by Noble.[11] Both procedures are extremely time-consuming. Also, since inverse of large matrices must be evaluated, they are extremely susceptible to numerical error. Therefore, the present method eliminates much unnecessary labor and source for numerical error associated with such inversions.

Results and Discussion

The problem considered in the foregoing analysis contains several parameters: τ_o, N, Pe, Ar, G, ε_w, ω_o, θ_e, θ_1, and θ_2. Numerical solutions were generated for various combinations of the above parameters. All computations were performed in double precision on IBM 370/3033.

The results presented here were obtained using an 11×11 grid. Further spatial subdivision of the enclosure did not yield more accurate results. Convergence was checked using a tolerance of 0.0001 on the temperature. The numerical algorithm was started by an initial guess for the temperature field. During the parametric study, whenever possible, results of previous cases were used as initial estimates to generate new solutions, otherwise a "zero fill" was used as the initial guess. Approximately 1 min CPU was required to generate the

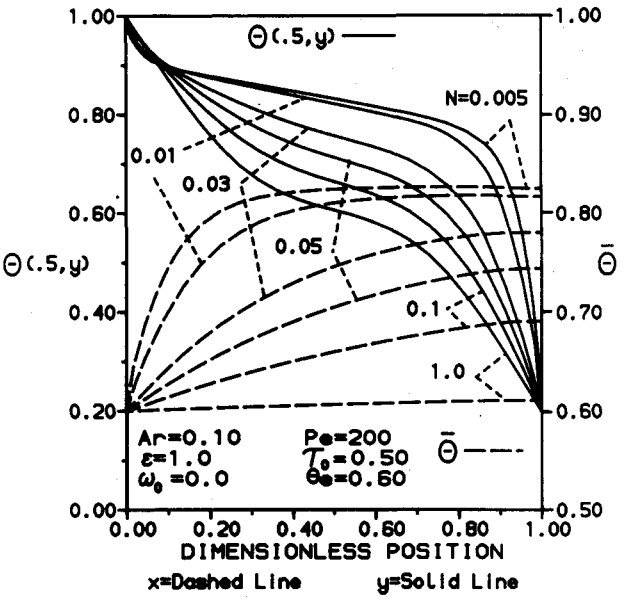

Fig. 3 Effect of conduction-radiation parameter on the temperature profiles. Dimensionless position: x = dashed line, y = solid line.

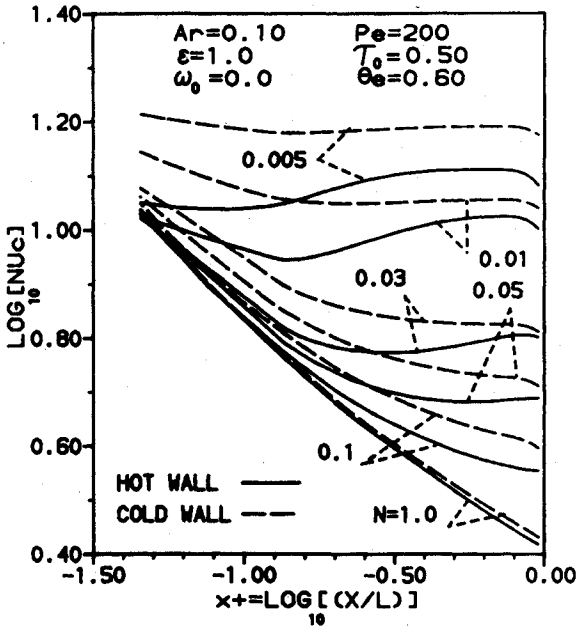

Fig. 4 Effect of conduction-radiation parameter on the local convective Nusselt number.

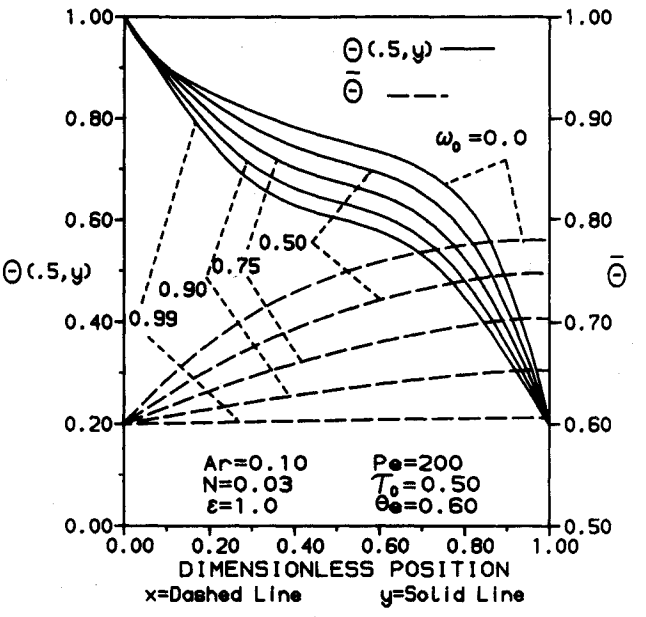

Fig. 5 Effect of scattering albedo on the temperature profiles. Dimensionless position: x = dashed line; y = solid line.

direct exchange factors. In general, solutions of the transport equations were generated in less than 2 min CPU time. As mentioned before, an interesting feature of the present method is that scattering and multiple reflection results were generated with the same computational effort as nonscattering black surface cases.

To check the accuracy of the computational scheme, several limiting cases of the present problem were examined and compared with solutions available in the literature. In the limit $\tau_0 = 0.0$, solutions were compared to that of Sellers[12] for pure convective flows between parallel plates. The results for combined convecting and radiating flow of a nonscattering gas in a black channel were checked against Kurosaki[13] for different values of Pe number. Another case considered was radiative heat transfer of a uniformly heat-generating gas ($N = 0.0$, $G = 4.0$) in a rectangular enclosure where effects of scattering on the temperature distributions and wall heat fluxes, at ω_o values of 0.0, 0.5, and 0.75, were compared to that of Larsen.[14] Finally, to examine the effect of diffuse gray reflection at the walls, comparisons were made to Larsen's results[15] for pure radiative transfer in a rectangular enclosure with wall emissivities of 0.1, 0.5, and 0.9. In all the above cases, agreement was found to be excellent with differences of less than 1%.

During the course of this investigation a complete parametric study was performed. However, since nine independent parameters are involved, presentation of the complete parametric study is not feasible. Only the cases where $\theta_1 = 1.0$, $\theta_2 = 0.2$, $\theta_e = 0.6$, $G = 0$, and ε_1 and $\varepsilon_2 = \varepsilon$ are presented here. In order to reveal important heat-transfer characteristics of the process, the effects of N, ε, ω_o, and Ar on the temperature distributions in the fluid and heat transfer at the hot and cold walls are emphasized. The magnitude of the other parameters are chosen so that strong interaction between conductive, convective, and radiative mechanisms is ensured. Results generated for a range of Pe and τ_o values are presented in Ref. 10.

The effect of conduction-radiation parameter on the temperature profiles in the fluid is shown in Fig. 3. As indicated, in the limit $N = 1.0$ when radiation is negligible compared to convection, the mixed mean temperature of the fluid rises very little above the inlet temperature. When the effect of radiation is increased with decreasing N, the temperature of the medium rises more rapidly and tends to level near the end of the

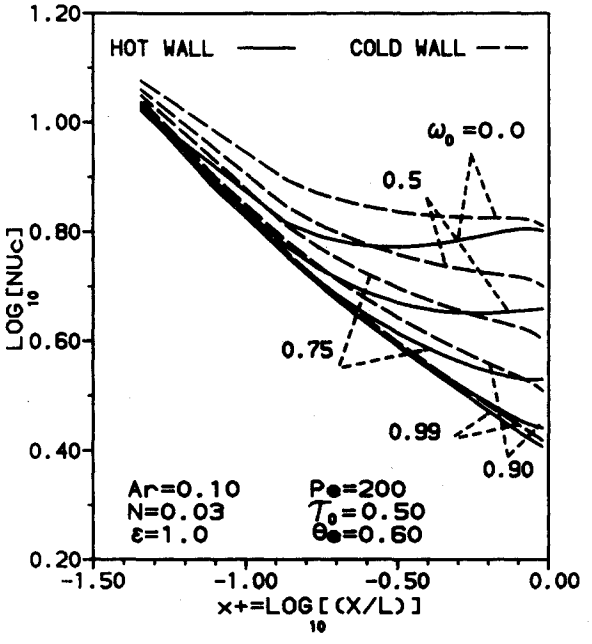

Fig. 6 Effect of scattering albedo on the local convective Nusselt number.

channel. At $N = 0.005$, which corresponds to almost pure radiative transfer, the mixed mean temperature in the fluid rises very fast, approaching a plateau of uniform temperature at the middle of the channel. This behavior is a result of heat-transfer augmentation caused by the radiation process, and it is clear that the effect of the hot wall is predominant.

Note that this trend, which is also reported in Ref. 1, is a direct outcome of the fact that the temperature of the outlet reservoir is represented by the mixed mean temperature of the fluid at the exit. In an open pipe situation where temperature θ_o is prescribed and lower than the average fluid temperature, a drop in the fluid temperature is predicted.

A study of the transverse profiles at the location $x = 0.5$ in the channel reveals that as the effect of radiation increases, the

temperature in the midsection of the channel rises and becomes more uniform. This is accompanied by sharper temperature changes near the two walls. Note also that the conduction-convection process ensures the continuity of temperature at the walls. Near the hot wall, more radiant energy is emitted by the fluid than absorbed. This sink effect must be compensated by the convection-conduction process. Near the cold wall, more radiant energy is absorbed by the fluid than emitted. Again, this radiative heating must be balanced by convective transfer to the wall. The increase in temperature gradients near the wall at decreasing N can, therefore, be explained physically by the fact that increased radiative heating of the medium near the cold wall must be congruent with increased convective cooling by that wall. Similarly, the increased sink effect near the hot wall must be compensated by increased convective heating at that boundary. As a result, an increase in radiation increases convective flux at both walls.

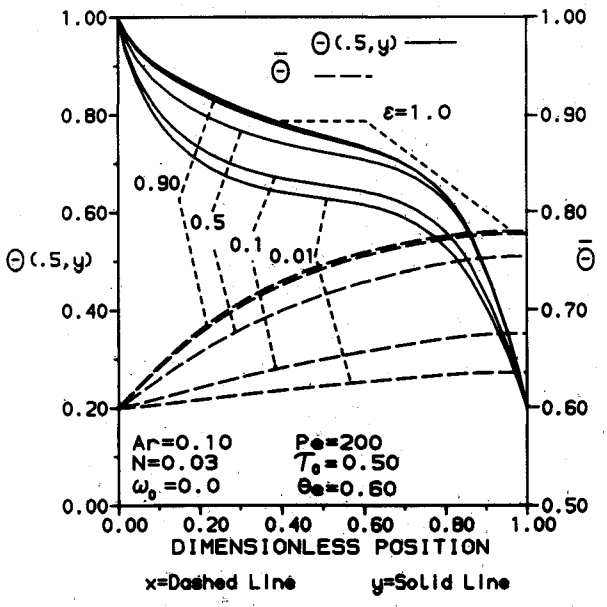

Fig. 7 Effect of wall emissivity on the temperature profiles. Dimensionless position: x = dashed line, y = solid line.

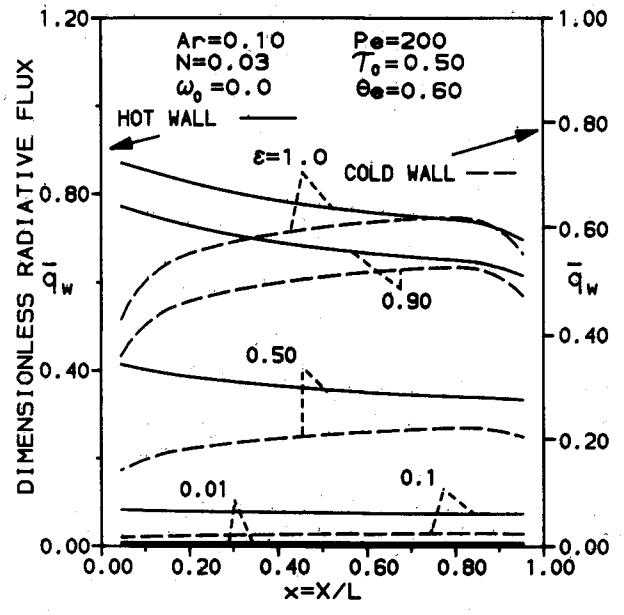

Fig. 8 Effect of wall emissivity on the net radiative flux.

The augmentation effect of radiation on convection is also seen in Fig. 4 where it is confirmed that with a decrease in N, the magnitude of convective Nusselt number Nu_c increases at any position in the channel. At large values of N when radiation effects are weak, the behavior of Nu_c for both the cold and hot walls is similar in its approach to an asymptotic value to pure convective flows. This trend changes with a decrease in N. At the hot wall for small N when the effects of radiation are strong, a point of minimum is reached beyond which any increase in Nu_c is not due to additional heat flux, but due to the state of relative thermal uniformity in the medium. This state is achieved when temperature of the fluid away from the walls become uniform, and the difference between the mixed mean temperature and the temperature of

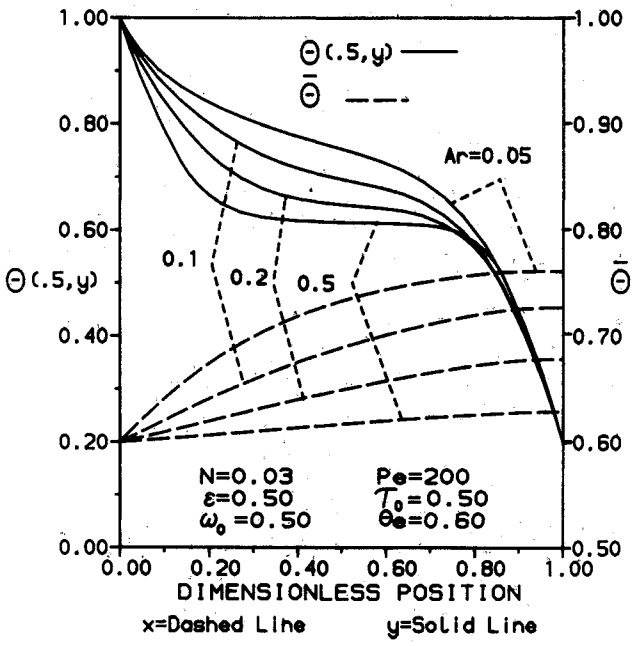

Fig. 9 Effect of aspect ratio on the temperature profiles. Dimensionless position: x = dashed line, y = solid line.

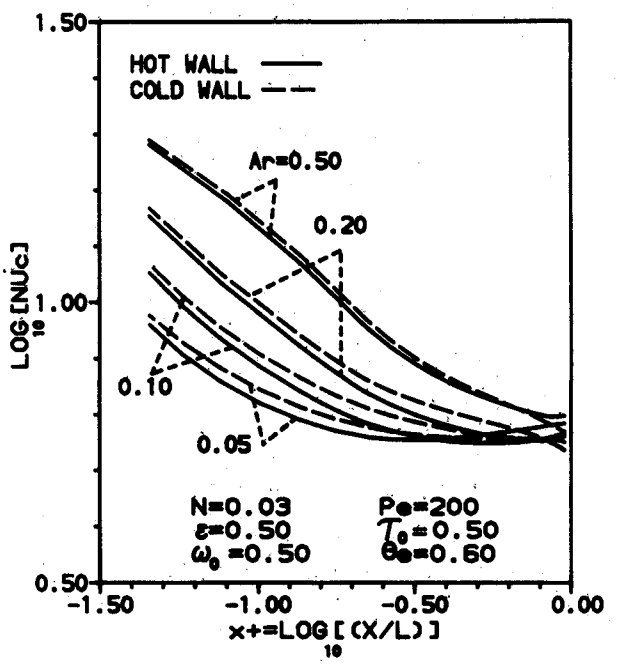

Fig. 10 Effect of aspect ratio on the local convective Nusselt number.

the hot wall diminishes. Note that with a decrease in N, the location and magnitude of small Nu_c changes, occurring more and more toward the inlet. Therefore, through redistribution of heat, radiation tends to promote thermal uniformity in the medium.

A look at Nu_c for the cold wall reveals a slightly different behavior. Since the thermal uniformity in the medium is promoted by the temperature at the hot wall, the difference between mixed temperature and the temperature of the cold wall increases along the channel. As a result, a minimum Nu_c similar to the one for the hot wall does not occur. At very low N values there is a slight rise in Nu_c. But a study of heat-flux distributions indicates that this rise is, indeed, due to increased convective cooling which has to compensate for increased radiative heating of the fluid near the cold wall. As the effect of radiation decreases, more similar behavior is observed for Nu_c at the top and bottom walls. At $N = 1.0$, the results are almost identical.

The effect of single scattering albedo on the temperature profiles in the fluid is shown in Fig. 5. It is evident that increased scattering in the medium diminishes the effect of radiation on the temperature profiles. When $\omega_o = 0.99$, the energy equation is almost completely decoupled from the radiative transfer equation, and the temperature profiles are similar to that of pure convection. Note also that an increase in scattering decreases by reducing the effect of radiation and, therefore, reduces the temperature gradients and convective heat fluxes at the walls.

This is also evident in Fig. 6 where it is observed that an increase in ω_o decreases the convective Nusselt numbers at both walls and delays the occurrence of minimum Nu_c along the hot wall. It is also interesting to notice the similarity between Nu_c curves for $\omega_o = 0.99$ and $N = 1.0$ in Figs. 4 and 6, respectively; both correspond to convection-dominated situation.

Figure 7 demonstrates the effect of wall emissivity on the temperature distributions in the medium. It is apparent that black boundaries cause the largest radiation effect and, therefore, the greatest heat-transfer augmentation in the fluid. It is also indicated that as surface emissivity decreases, the temperature of the fluid near the hot boundary drops due to the reduced emission by that wall. Consequently, more drastic temperature gradients are displayed near the hot wall.

The net radiative heat fluxes at the hot and cold walls are shown in Fig. 8. In both cases, as expected, radiative heat flux decreases with a decrease in emissivity. For the hot wall, the greatest radiative flux occurs at the inlet due to the large heat loss to the cold inlet reservoir. Radiative flux then decreases with distance along the channel. This is true for all values of emissivity. For the cold wall, however, the maximum radiative flux occurs in the inner sections of the channel, close to the outlet. Most of the incoming radiative energy from the fluid is directed toward this section. At $\varepsilon = 0.01$, the wall surfaces becomes almost pure reflectors, and the net radiative flux is negligible. In this case, energy is transported from the walls only by conduction. The distributive action of radiation in this instance is to only change the total energy flux in the stream. However, the local energy flux does not vanish and, thus, the temperature profile shown in Fig. 7 still differs from that of pure convection.

The influence of aspect ratio on the temperature distributions and heat-transfer characteristics of a scattering medium in a reflecting channel is shown in Figs. 9 and 10. From Fig. 9 it can be ascertained that the closer the walls of channel are, the greater the effect of radiation on the profiles. It is also observed that the impact of Ar on the temperature profile is more pronounced near the hot wall, whereas the temperature of the fluid near the cold wall is relatively unaffected by changes in Ar.

Finally, the effect of aspect ratio on the convective heat transfer can be studied from Fig. 10. Here it is revealed that the further the walls of the channel are from each other, the greater is the contribution of convective heat transfer. If the channel walls are close, the hot wall has more influence in raising the mixed mean temperature in the fluid. Thus, as aspect ratio decreases, the location of minimum Nu_c shifts more toward the inlet of the duct.

Conclusion

Combined two-dimensional convective and radiative heat transfer from a gray medium in a rectangular channel was studied. The resulting set of simultaneous integro-partial differential equations were solved numerically using an element-to-node approach. The numerical scheme was found to be simple, accurate, and efficient. It is ideally suited for combined heat-transfer problems, especially in situations that include radiative scattering and reflection. From the cases examined the following conclusions are drawn.

1) When radiation interacts with convection, larger temperature gradients develop near the hot and cold walls. Therefore, interaction of radiation with convection increases convective heat flux and, in general, results in the augmentation of the heat-transfer process.

2) The interaction process is significantly influenced by ω_o, ε, and Ar. Scattering in the fluid reduces the role of radiation, and black walls produce the largest radiation effect.

3) Because of the presence of radiation, the behavior of convective Nusselt number at the hot and cold walls is different. Nu_c at the two walls become identical only at large N and ω_o values when convection is dominant.

4) At the hot wall when radiation is strong, Nu_c goes through a minimum, beyond which an increase in Nu_c is caused by the small difference between the wall temperature and the mixed mean temperature of the medium and is not due to additional heat flux.

5) The position and magnitude of the minimum Nu_c and, thus, the thermal uniformity in the fluid, are significantly affected by the different parameters of the problem.

Appendix A: Direct Exchange Areas

The radiative exchange quantities present in Eqs. (2c) and (3c) can be written using Bouger's law of transmittance:

$$\frac{1}{k_t}\frac{\partial^2 g_\mu g_\gamma}{\partial V_\mu \partial V_\gamma} = \frac{k_t e^{-k_t|\boldsymbol{R}_\gamma - \boldsymbol{R}_\mu|}}{\pi|\boldsymbol{R}_\gamma - \boldsymbol{R}_\mu|^2} \tag{A1}$$

2) wall or surface to fluid exchange

$$\frac{1}{k_t}\frac{\partial^2 w_\alpha g_\gamma}{\partial A_\alpha \partial V_\gamma} = \frac{1}{k_t}\frac{\partial^2 s_\alpha g_\gamma}{\partial A_\alpha V_\gamma} = \frac{\cos\phi_\alpha e^{-k_t|\boldsymbol{R}_\gamma - \boldsymbol{R}_\alpha|}}{\pi|\boldsymbol{R}_\gamma - \boldsymbol{R}_\alpha|^2} \tag{A2}$$

3) fluid to wall exchange

$$\frac{\partial^2 g_\mu w_\pi}{\partial V_\mu \partial A_\pi} = \frac{k_t \cos\phi_\pi e^{-k_t|\boldsymbol{R}_\pi - \boldsymbol{R}_\mu|}}{\pi|\boldsymbol{R}_\pi - \boldsymbol{R}_\mu|^2} \tag{A3}$$

4) wall or surface to wall exchange

$$\frac{\partial^w s_\alpha w_\pi}{\partial A_\alpha \partial A_\pi} = \frac{\partial^2 w_\alpha w_\pi}{\partial A_\alpha \partial A_\pi} = \frac{\cos\phi_\alpha \cos\phi_\pi e^{-k_t|\boldsymbol{R}_\pi - \boldsymbol{R}_\alpha|}}{\pi|\boldsymbol{R}_\pi - \boldsymbol{R}_\alpha|^2} \tag{A4}$$

where subscripts γ and π represent receiving differential volume and area, and μ and α represent sending volume and area.

The above exchange terms can be integrated over the volume or area elements to give element-to-node direct exchange integrals presented in Table 1. Because of the nonuniformity of temperature and radiative flux in each element, additional variations to these fundamental exchange integrals are needed [see Eqs. (11b), (11c)]. As an example for the case

of fluid to fluid exchange, we have

$$\overline{g_{mn}g_{ij}}' = \frac{2k_t}{\pi\eta_o}\int_{-\eta_o/2}^{\eta_o/2}\int_{-\xi_o/2}^{\xi_o/2}\eta\frac{F_1(k_t,s)}{s}\,d\xi\,d\eta \qquad (A5)$$

$$\overline{g_{mn}g_{ij}}'' = \frac{2k_t}{\pi\xi_o}\int_{-\eta_o/2}^{\eta_o/2}\int_{-\xi_o/2}^{\xi_o/2}\xi\frac{F_1(k_t,s)}{s}\,d\xi\,d\eta \qquad (A6)$$

$$\overline{g_{mn}g_{ij}}''' = \frac{2k_t}{\pi\eta_o\xi_o}\int_{-\eta_o/2}^{\eta_o/2}\int_{-\xi_o/2}^{-\xi_o/2}\eta\xi\frac{F_1(k_t,s)}{s}\,d\xi\,d\eta \qquad (A7)$$

the quantities

$$\overline{w_n g_{ij}}', \quad \overline{g_{mn}w_i}', \quad \overline{g_{mn}w_i}'', \quad \overline{g_{mn}w_i}''', \quad \overline{w_n w_i}'$$

are similarly defined. The integration in the above expressions were performed numerically over the η-ξ domain.

References

[1]Chung, T. J. and Kim, J. Y., "Two-Dimensional, Combined Mode Heat Transfer by Conduction, Convection, and Radiation in Emitting, Absorbing and Scattering Media-Solution by Finite Elements," *Journal of Heat Transfer*, Vol. 106, 1984, pp. 448–452.

[2]Chawla, T. C. and Chan, S. H., "Combined Radiation, Convection in Thermally Developing Poiseuille Flow with Scattering," *Journal of Heat Transfer*, Vol. 102, 1980, pp. 297–302.

[3]Azad, F. H. and Modest, M. F., "Combined Radiation and Convection in Absorbing, Emitting and Anisotropically Scattering Gas-Particulate Tube Flow," *International Journal of Heat Mass Transfer*, Vol. 24, 1981, pp. 1681–1697.

[4]Smith, T. F., Ki-Hong Byun, and Ford, M. J., "Heat Transfer for Flow of an Absorbing, Emitting, and Isotropically Scattering Medium Through a Tube with Reflecting Walls," *Heat Transfer 1986*, Hemisphere Publishing, Vol. 2, 1986, pp. 803–808.

[5]Modest, M. F., "Radiative Equilibrium in a Rectangular Enclosure Bounded by Gray Walls," *J. Quant. Spectrosc. Radiat. Transfer*, Vol. 15, No. 6, 1975, pp. 445–461.

[6]Kobiyama, M., Taniguchi, H., and Saito, T., "The Numerical Analysis of Heat Transfer Combined with Radiation and Convection," *Bulletin of JSME*, Vol. 22, No. 267, 1979, pp. 707–714.

[7]Hottel, H. C. and Sarofim, A. F., *Radiative Transfer*, McGraw-Hill, New York, 1964.

[8]Fiveland, W. A., "Discrete Ordinates Solutions of the Radiative Transport Equation For Rectangular Enclosures," *Journal of Heat Transfer*, Vol. 106, 1984, pp. 699–706.

[9]Kassemi, M. and Chung, B. T. F., "Conjugated Heat Transfer of a Radiatively Participating Gas in a Channel," *Heat Transfer 1986*, Hemisphere Publishing, Vol. 2, 1986, pp. 797–802.

[10]Kassemi, M., "Conjugated Heat Transfer from a Radiating Gas in a Channel," Ph.D Dissertation, Dept. of Mechanical Engineering, University of Akron, Akron, OH, 1987.

[11]Noble, J., "The Zone Method: Explicit Matrix Relations For Total Exchange Areas," *International Journal of Heat Mass Transfer*, Vol. 18, 1975, pp. 261–269.

[12]Seller, J. R., Tribus, M., and Klein, J. S., "Heat Transfer Laminar Flow in a Round Tube or Flat Conduit—The Graetz Problem Extended," *Transactions of the ASME*, Vol. 78, No. 2, 1956, pp. 441–448.

[13]Kurosaki, Y., "Heat Transfer by Simultaneous Radiation and Convection in an Absorbing and Emitting Medium in a Flow Between Parallel Plates," *Proceedings of the Fourth International Heat Transference Conference*, Paris, Vol. R 2.5., 1970.

[14]Larsen, M. E., "The Exchange Factor Method: An Alternative Zonal Formulation for Analysis of Radiating Enclosures Containing Participating Media," Ph.D. Dissertation, University of Texas at Austin, Austin, TX, 1983.

[15]Larsen, M. E. and Howell, J. R., "The Exchange Factor Method: An Alternative Zonal Formulation of Radiating Enclosure Analysis," American Society of Mechanical Engineers, Paper 82-WA/HT-50, 1982.